

# Properties of extra-planar H I clouds in the outer part of the Milky Way.

L. Dedes<sup>1,2</sup> and P.W.M Kalberla<sup>1</sup>

<sup>1</sup> Argelander Institut für Astronomie, Universität Bonn, Auf dem Hügel 71, 53121 Bonn

<sup>2</sup> Max-Planck-Institut für Radioastronomie, Auf dem Hügel 69, 53121 Bonn  
e-mail: ldedes@astro.uni-bonn.de, pkalberla@astro.uni-bonn.de

Received —; accepted —

## ABSTRACT

*Context.* There is mounting evidence for an extra-planar gas layer around the Milky Way disk, similar to the anomalous H I gas detected in a few other galaxies. As much as 10% of the gas may be in this phase.

*Aims.* We analyze H I clouds located in the disk-halo interface outside the solar circle to probe the properties of the extra-planar H I gas, which is following Galactic rotation.

*Methods.* We use the Leiden/Argentine/Bonn (LAB) 21-cm line survey to search for H I clouds which take part in the rotation of the Galactic plane, but are located above the disk layer. Selected regions are mapped with the Effelsberg 100-m telescope. Two of the H I halo clouds are studied in detail for their small scale structure using the Westerbork Synthesis Radio Telescope (WSRT)\* and the NRAO Very Large Array (VLA)\*\*.

*Results.* Data from the 100m telescope allow for the parameterization of 25 distinct H I halo clouds at Galactocentric radii 10 kpc <  $R$  < 15 kpc and heights 1 kpc <  $z$  < 5 kpc. The clouds have a median temperature of 620 K, column densities of  $N_{\text{HI}} \sim 10^{19} \text{ cm}^{-2}$ , and most of them are surrounded by an extended envelope of warmer H I gas. Interferometer observations for two selected regions resolve the H I clouds into several arc-minute sized cores. These cores show narrow line widths ( $\Delta v_{1/2} \sim 3 \text{ km s}^{-1}$ ), they have volume densities of  $n > 1.3 \text{ cm}^{-3}$ , masses up to  $24 M_{\odot}$ , and are on average in pressure equilibrium with the surrounding envelopes. Pressures and densities fall within the expectations from theoretical phase diagrams ( $P$  vs  $\langle n_h \rangle$ ). The H I cores tend to be unstable if one assumes a thermally bistable medium, but are in better agreement with models that predict thermal fragmentation driven by a turbulent flow.

**Key words.** Galaxy: halo - radio lines: ISM - ISM: clouds

## 1. Introduction

The H I gas is a major constituent of the interstellar medium (ISM), and it is a well known property of this gas that it settles in the Galactic plane. From the very first H I observations it is also known that the disk gas is co-rotating with the stellar disk. Taking both properties together one may use the gas distribution to describe the morphology of the Galactic disk.

As yet, there is no sharp boundary for the disk emission. Oort (1962) was the first who mentioned this fact. “Well outside the real disk one still finds neutral hydrogen with an average density of between 5 and 10 per cent of the intensities one observes in the plane”. Oort was referring to observations with the Dwingeloo telescope, and Shane (1967) described this gas later as a “galactic envelope”, a smooth envelope of neutral hydrogen surrounding the spiral structure, following the same Galactic rotation as the gas in the plane. Further discussion of this envelope was given by Takakubo (1967) and by Shane (1971), but there was some concern about a possible contamination by stray radiation from the antenna diagram of the Dwingeloo telescope.

Send offprint requests to: L. Dedes

\* The Westerbork Synthesis Radio Telescope is operated by ASTRON (Netherlands Foundation for Research in Astronomy) with support from the Netherlands Foundation for Scientific Research NWO.

\*\* The National Radio Astronomy Observatory is a facility of the National Science Foundation operated under cooperative agreement by Associated Universities, Inc.

The extra-planar gas component was also visible in the Weaver & Williams (1973) survey, and Lockman (1984) studied this feature in some more detail. Supplementing observations were made with the NRAO 300-foot telescope and came also from the NRAO 140-foot survey by Burton & Liszt (1983). Lockman argued that his analysis was not affected by stray radiation. He found for Galactocentric radii  $4 \lesssim R \lesssim 8$  kpc that 13% of the H I gas is located outside the disk, extending to  $z$ -distances of 1 kpc or more and termed this component an “H I halo”.

The Bell Labs survey (Stark et al. 1992) is only little affected by instrumental effects, and Lockman & Gehman (1991) used this survey to analyze the nature of the vertical H I gas distribution in the direction of the Galactic poles. They proposed for the H I gas a decomposition in several layered structures, corresponding to distinct different isothermal cloud populations. The scale height for each component results from the pressure balance of a cloudy turbulent medium against the gravitational potential of the Milky Way. The concept of a layered structure of the H I contains essentially three components: a cold neutral medium (CNM), a warm neutral medium (WNM) and an extra-planar component (Dickey & Lockman 1990) which is often called “Lockman Layer”.

The layer concept is based on the average emission from the extra-planar H I gas layer which is very faint. The clumpy nature of the H I gas implies then that extra-planar H I clouds must have a low volume filling factor. The layer concept describes therefore an ensemble of H I clouds or the probability distribution of such objects. First indications for a population of such

clumps were found by Simonson (1971). These early data came from the Dwingeloo telescope. Almost three decades later the Leiden/Dwingeloo survey (LDS, (Hartmann & Burton 1997)) became available and provided a much improved database, more sensitive and essentially free of stray radiation. Channel maps show numerous clumps and filaments that are detached from the disk, and Kalberla et al. (1998) argued for an extra-planar gas layer which can be characterized by a distribution with a velocity dispersion of  $\sigma = 60 \text{ km s}^{-1}$ , considerably larger than the dispersion suggested by Lockman & Gehman (1991).

The first high resolution data of the extra-planar gas layer at a beam-width of  $9'$  have been taken by Lockman (2002) with the Robert C. Byrd Green Bank Telescope (GBT). These observations demonstrated convincingly the nature of the extra-planar gas layer as a population of cold clumps with a typical mass of  $50 M_{\odot}$ . Many of these clumps appear to be surrounded by warmer envelopes. A larger sample of clouds in the lower halo was studied by Ford et al. (2008) with the Parkes Telescope. These clumps are somewhat larger and more massive than the sample detected by Lockman (2002). This cloud population, located close to  $R \sim 3.8 \text{ kpc}$ , is interpreted as originating from a Galactic fountain. Such a model would also explain the high kinetic energy which is needed for individual clouds to reach large  $z$ -distances. Support for such an interpretation comes from Stil et al. (2006). They found fast moving clumps in the Galactic plane with velocity vectors located *within* the Galactic plane, analogous to fast velocities *perpendicular* to the plane as suggested as an explanation for the extra-planar gas layer.

So far we discussed predominantly Galactocentric distances  $R \lesssim 8.5 \text{ kpc}$ , where  $8.5 \text{ kpc}$  is the I.A.U Sun–Galactic center distance, since most of the observations are in this range. For a more general description of this phenomenon, in particular for the question whether the extra-planar gas layer is caused by a fountain flow, objects at larger distances are needed. Kalberla & Dedes (2008) argue that extra-planar gas is present even at  $R \gtrsim 35 \text{ kpc}$ . Gas at such distances can hardly originate from fountain events.

Direct evidence for a population of extra-planar H I clouds outside the Solar circle was first given by Stanimirović et al. (2006). Arecibo data in the direction towards the anti-center suggest that these clouds are not restricted to the inner part of the Milky Way disk, which is similar to preliminary results with the Effelsberg telescope reported by Kalberla et al. (2005). In the following we intend to explore the extra-planar gas layer of the outer part of the Milky Way in some more detail. Our results are based on single-dish observations with the Effelsberg 100-m radio telescope and on interferometer observations with the VLA and the WSRT array.

This paper is organized as follows. In Sect. 2 we explain our selection criteria for targets that have been mapped with the 100-m telescope. Our observations are described in Sect. 3. We discuss the properties of the H I cloud sample detected by us with the 100-m telescope, and also the results from two targeted interferometer observations in Sect. 4. We find evidence for a multi-phase structure and compare in Sect. 5 the derived physical parameters with theoretical models. Sect. 6 gives our summary and conclusion.

## 2. Methods

Extra-planar H I clouds are known to have a patchy distribution. Accordingly, a strategy is needed for a successful search. If one likes to measure “gas well outside the real disk” (Oort 1962), the first step is obviously to determine the extension of the disk.

Next, one needs to search in regions above the disk. For the inner part of the Galaxy the approach is easy. The scale height of the gas is approximately constant for  $3 \lesssim R \lesssim 8 \text{ kpc}$ , the boundary between disk and halo is well defined. 13% of the gas resides at  $|z| > 500 \text{ pc}$  with little fluctuations for  $4 \lesssim R \lesssim 8 \text{ kpc}$  (Lockman 1984).

For the outer part of the Milky Way the situation is more complex. The gas flares strongly, and in addition the disk is significantly warped. Both cannot be disregarded, and it is necessary to obtain good estimates for the mid-plane position and the scale height of the H I gas. Two groups have recently independently determined the shape of the H I gas distribution, Levine et al. (2006) and Kalberla et al. (2007). Their results are in good agreement, and we adopt the disk parameters as derived by Kalberla & Dedes (2008), which were previously also used by Kalberla et al. (2007) for a determination of the average extra-planar gas fraction. On average 10% of the H I gas is located outside the disk, the extra-planar gas is well defined for  $8.5 \lesssim R \lesssim 22 \text{ kpc}$ , but tends to increase toward smaller radii  $R$ , consistent with the determination by Lockman (1984). We conclude that a search for extra-planar H I clouds in the outer part of the Milky Way should be promising for  $R \lesssim 22 \text{ kpc}$  if warp and flaring are taken into account.

### 2.1. H I halo cloud selection

We used the Kalberla & Dedes (2008) model to calculate the expected emission  $t_{ex}(l, b, v)$  for extra-planar gas and  $t_{disk}(l, b, v)$  respectively for disk gas. The ratio  $t_{ex}(l, b, v)/t_{disk}(l, b, v)$  defines a probability that a cloud feature, observed at position  $l, b$  with the velocity  $v$  may belong to the extra-planar gas layer. The extra-planar gas layer is patchy, and we therefore searched the Leiden/Argentine/Bonn (LAB) survey (Kalberla et al. 2005) for positions containing weak H I emission that may originate from clouds in the lower halo.

We tested our method in the inner part of the Milky Way and recovered those regions that have been observed previously by Lockman (2002) and Ford et al. (2008) as the ones that are most promising for a detection of extra-planar gas clumps. After this successful test we applied our search algorithm to  $R \gtrsim 8.5 \text{ kpc}$ .

### 2.2. Distance determination

Quantities directly observable for H I clouds are: column density  $N_{\text{HI}}$ , angular size of the cloud  $s$  and line width  $\Delta v_{1/2}$ . The cloud diameter  $D$ , the average spatial volume density  $\langle n \rangle$ , pressure  $P$  and visible mass  $M_{\text{HI}}$  can be determined only if the distance  $d$  of the cloud is known. Since the regions probed by us are outside the solar circle, a Milky Way velocity field needs to be used to convert the line-of-sight velocity  $v_{lsr}$  of a cloud to its distance  $d$ . We use a mass model and a rotation curve according to Kalberla et al. (2007), which assumes that the halo gas is slightly lagging behind the Galactic disk. Assuming co-rotation would lead to deviations of 6–22% depending on the region. For the Brand & Blitz (1993) rotation curve, differences would amount to 15–30%. Finally, in comparison with the Milky Way model from Gómez (2006) the deviation for the distance determination is between -7% and -14%. All together, distances determined by us may have typical systematical uncertainties of about 15–20%.

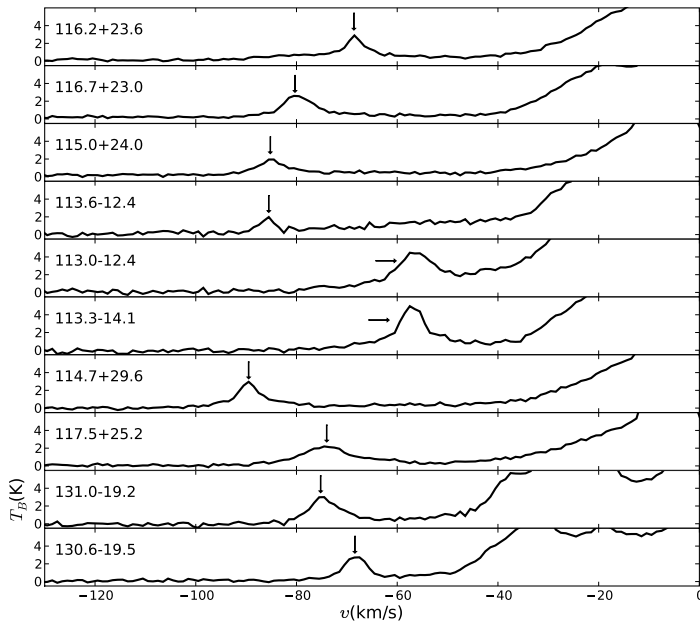


**Fig. 1.** Spectra of H I clouds detected using the Effelsberg telescope. Arrows mark the position of the H I clouds in the spectra. The main galactic line is visible at the right side of the plot. The extending wings are seen up to  $\sim 100 \text{ km s}^{-1}$ , underlying the H I clouds.

### 3. Observations

#### 3.1. Effelsberg observations

22 fields, each covering  $3^\circ \times 3^\circ$ , could be observed with the 100-m Effelsberg telescope. All the fields have a longitude of  $l > 90^\circ$ , and the selection was based on the criteria described in Sect. 2. Therefore we are confident that the H I emission is associated with the neutral component of the gaseous halo. The observations were done during the period from May 2004 to October 2005. We used the AK-90 auto-correlator with two polarizations at a bandwidth of 10 MHz with 2048 channels. This results in a channel separation of 4 kHz (velocity separation  $0.84 \text{ km s}^{-1}$ ) and velocity resolution  $1.03 \text{ km/s}$ . The fields were mapped beam-by-beam on a  $9'$  grid. The integration for each position was 60 sec. For a system temperature  $T_{\text{sys}} = 27 \text{ K}$  this implies a sensitivity of  $\sigma_n = 0.1 \text{ K}$ . The Effelsberg data were calibrated using the IAU standard position S7 (Kalberla et al. 1982). A first order polynomial was applied to correct the baseline, and the stray radiation contamination was removed using the method by Kalberla et al. (1980). The final result was an image cube with a  $9'$  angular resolution and  $1 \text{ km s}^{-1}$  velocity resolution. To verify the observations, the detected H I clouds were re-observed using a full sampling ( $4.5'$  grid). The configuration of the AK-90 auto-correlator was identical. The integration was increased to 90 sec per position, resulting in a theoretical sensitivity of  $\sigma_n = 0.08 \text{ K}$ .

#### 3.2. Synthesis array observations

After extracting a sample of the H I halo clouds from the Effelsberg data (see Sect. 4.1), follow-up observations were made for two of the clouds with the WSRT and the VLA synthesis arrays.

The cloud at  $l, b = 116.2^\circ, 23.6^\circ$  at  $v_{\text{lsr}} = -68 \text{ km s}^{-1}$  was observed with the WSRT array, mapping the region at (J2000)

$\alpha, \delta = 20^{\text{h}}4^{\text{m}}22^{\text{s}}, 82^{\text{d}}56'36''$  in a maxi-short configuration. The integration time was 12 hours. A double IF was used with a bandwidth of 2.5 MHz and 1024 channels. This backend configuration results in a channel separation of 2.5 kHz and a velocity separation of  $0.5 \text{ km s}^{-1}$ . The data were reduced with the MIRIAD<sup>1</sup> software package. For flux calibration the source 3C286 was used, while self-calibration was applied to correct the phase errors. The dirty cube has a sensitivity of  $\sigma_n \sim 2.25 \text{ mJy/beam}$ . After applying continuum subtraction, the dirty cube was deconvolved using the Clark CLEAN algorithm (Clark 1980) and convolved with a Gaussian beam. The final result is an image cube with a  $60''$  resolution and  $1 \text{ km s}^{-1}$  velocity resolution.

The cloud at  $l, b = 115.0^\circ, +23.9^\circ$  and  $v_{\text{lsr}} = -84.50 \text{ km s}^{-1}$  was observed with the VLA array mapping the region (J2000)  $(\alpha, \delta) = 20^{\text{h}}29^{\text{m}}, 82^{\text{d}}08'$  for six hours in the DnC configuration. A double IF was used with a bandwidth of 0.78 MHz and 256 channels in each IF. With this configuration we have a channel separation of 3.05 KHz resulting in a velocity separation of  $0.64 \text{ km s}^{-1}$ . The data were reduced using the NRAO Astronomical Image Processing System (AIPS)<sup>2</sup>. The source 3C286 was used as a flux calibrator and the close-by source 2344+824 as a phase calibrator. The dirty cube has a sensitivity of  $\sigma_n \sim 2.25 \text{ mJy/beam}$ . The dirty image was deconvolved using the Clark CLEAN algorithm (Clark 1980) after the continuum subtraction. The clean components were restored with a Gaussian beam, resulting in a clean image with a  $60''$  resolution.

## 4. Results

### 4.1. Single dish

The total area covered by the 22 fields observed with the 100-m telescope is  $\sim 204 \text{ deg}^2$ . Due to the diffuse nature of the clouds it was not possible to use automated detection algorithms, so the selection was done manually. Application of the criteria discussed in Sect. 2.1 yielded 25 objects identified as H I halo clouds with line-of-sight velocities  $v_{\text{lsr}}$  close to the emission of the underlying disk. Fig. 1 shows a few examples of the observed line spectra. The lines are narrow but superposed on extended wings of diffuse Galactic H I emission. For the 100-m telescope, stray radiation effects have been taken into account; we are therefore confident that these observed components are not caused by instrumental effects.

Table 1 summarizes our single dish results. From the observed cloud position  $l, b$  and velocity  $v_{\text{lsr}}$  we derive its Galactocentric distance  $R$  and the height  $z$  above the plane (Kalberla & Dedes 2008). The angular diameter  $s$  is the geometrical mean of the major and the minor axis of the cloud. The high brightness temperature  $T_B$  of the clouds ensures that the effect of the noise is minimal. In some cases where the entry is missing in Table 1, the clouds were unresolved and the diameter could not be constrained due insufficient beam-by-beam measurements and because of the blending with the extended wings. The spatial diameter is calculated from  $s$  making use of the known distance. As mentioned in Sec. 2.2 this is one major source of uncertainties. Assuming optically thin gas, to obtain the line width  $\Delta v_{1/2}$  and the column density  $N_{\text{HI}}$  we tried to fit a one or two component Gaussian to the average spectrum of the cloud. In some clouds such as e.g. 116.2+23.6, 116.7+23.0 this was successful. In clouds like e.g. 113.0-12.4 and 113.3-14.1, where the extended wing was stronger, this was not possible.

<sup>1</sup> <http://www.atnf.csiro.au/computing/software/miriad/>

<sup>2</sup> <http://www.aips.nrao.edu/aips.faq.html>

**Table 1.** Properties of the observed H I halo clouds.

	$v_{lsr}$ km s <sup>-1</sup>	$R$ kpc	$z$ kpc	$N_{HI}$ 10 <sup>18</sup> cm <sup>-2</sup>	$s$ arcmin	$D$ pc	$\Delta v_{1/2}$ km s <sup>-1</sup>	$T_{kin}$ K	$\langle n \rangle$ cm <sup>-3</sup>	$P$ K · cm <sup>-3</sup>	$M_{HI}$ M <sub>⊙</sub>
113.3+27.0	-40	10.5	1.8	16(2)	13	16(7)	7.0	1080(150)	0.33(0.15)	360(170)	25(22)
113.2+25.5	-32	10.0	1.4	6(1)	9	8(5)	4.0	350(90)	0.23(0.14)	80(50)	3(4)
116.2+23.6	-68	12.5	2.8	11(2)	25	51(17)	3.0	200(70)	0.07(0.03)	14(8)	120(80)
116.7+22.8	-81	14.5	3.5	25(3)	27	70(19)	5.1	570(110)	0.12(0.04)	68(26)	770(440)
116.5+21.4	-42	10.5	1.5	36(4)	13	14(6)	5.4	650(120)	0.70(0.30)	455(210)	45(39)
115.0+23.9	-84	14.5	3.9	15(3)	22	60(20)	3.3	240(70)	0.08(0.03)	19(7)	220(140)
115.4+22.4	-66	12.0	2.5	35(3)	18	34(12)	10.0	2200(220)	0.33(0.12)	730(275)	260(180)
117.3+24.0	-71	13.0	3.0	36(3)	27	58(18)	8.1	1440(170)	0.20(0.06)	290(90)	770(490)
118.0+24.6	-71	13.0	3.1	20(3)	18	40(15)	5.0	550(110)	0.16(0.07)	87(40)	200(150)
118.0+24.0	-72	13.0	3.0	74(4)	18	40(15)	21.1	9800(460)	0.60(0.22)	5800(2140)	750(550)
117.5+25.2	-74	13.0	3.0	60(4)	18	40(15)	11.6	2960(260)	0.48(0.18)	1449(550)	600(440)
114.5-15.9	-38	10.5	-1.0	10(2)	18	18(7)	4	350(90)	0.18(0.08)	62(31)	20(16)
113.6-12.4	-85	4.5	-1.9	16(2)	13	35(14)	4	350(90)	0.14(0.06)	50(25)	120(100)
113.0-12.4	-55	12.0	-1.2	41(3)	18	28(9)	6.7	990(150)	0.49(0.16)	470(170)	205(130)
113.0-13.0	-40	10.5	-0.9	28(3)	9	9(5)	4.4	425(100)	1.02(0.32)	435(170)	14(16)
113.3-14.1	-57	12.0	-1.3	39(4)			4.9	510(100)			
113.6-13.5	-50	11.5	-1.3	68(5)			7.0	1080(150)			
114.3+21.8	-75	13.5	3.0	7(-)	9	21(12)					
128.8-18.5	-58	14.0	-1.9	54(6)			4.8	510(100)			
131.0-19.2	-72	15.0	-2.8	49(5)			5.4	640(120)			
130.6-19.5	-68	14.0	-2.5	35(3)			6.0	780(130)			
112.1+27.3	-39	10.5	1.8	6(1)	9	10(6)	5.3	620(120)	0.20(0.12)	126(80)	4(5)
113.8+28.7	-69	12.5	3.6	9(2)	18	39(14)	6.0	790(130)	0.08(0.03)	61(25)	90(70)
112.4+29.9	-65	12.5	3.7	4(1)	9	20(11)	2.0	80(40)	0.07(0.04)	6(5)	11(13)
114.7+29.6	-89	15.0	5.4	19(3)			3.6	285(80)			

Note -  $v_{lsr}$  is the line of sight velocity in km s<sup>-1</sup>,  $R$  is the Galactocentric distance.  $z$  is the height above mid-plane.  $N_{HI}$  is the H I column density.  $s$  is the measured angular diameter.  $D$  is the spatial diameter.  $\Delta v_{1/2}$  is the full width half maximum of the line width.  $T_{kin}$  the kinetic temperature.  $\langle n \rangle$  the volume H I density.  $P$  is the pressure of the H I gas.  $M_{HI}$  the visible H I mass of the cloud.

In those cases we had to first model the extended wing, then subtract it and estimate the  $\Delta v_{1/2}$  and the column density of the cloud. The observed line width  $\Delta v_{1/2}$  defines the upper limit for the kinetic temperature  $T_{kin}$  due to the effect of turbulence. For very cold clouds, assuming a spin temperature  $T_s = 80$  K, we expect the derived temperature not to be strongly biased, while for the broader lines the bias is larger. To determine the average volume density  $\langle n \rangle$ , we assumed a cylindrical shape:  $\langle n \rangle = N_{HI}/d$ . Deviations from this shape and the uncertainties in the distances determination are the major sources of biases in this estimate. The pressure was estimated from  $P = \langle n \rangle \cdot T_{kin}$ . This includes the thermal pressure as well as a turbulence component. Finally from the column density  $N_{HI}$  and size of the cloud  $D$  we estimated its visible mass using  $M = N_{HI} * D^2$ .

The Gaussian deconvolution of the clouds showed that most of them can best be fitted with a two-component Gaussian. This corresponds to a narrow compact component and to a broader more extended component. The best two examples which are present in this paper are the cloud 116.2+23.6 (Fig. 2) and 115.0+23.9. All the properties of the narrow components are given in Table 1 except the peak temperature, which for cloud 116.2+23.6 is  $T_C=1.8\pm 0.1$  K and for the cloud 115.0+23.9 is  $T_C=0.73\pm 0.1$  K. We estimated a peak temperature  $T_W=0.71\pm 0.1$  K, column density  $N_W=25\pm 4 \cdot 10^{18}$  cm<sup>-2</sup> and a  $\Delta v_{1/2}=18\pm 0.5$  km s<sup>-1</sup> for the broad component of the cloud 116.2+23.6. For the cloud 115.0+23.9 the Gaussian decomposition gave a peak temperature  $T_W=0.8\pm 0.1$  K, a column density  $N_W=20\pm 4 \cdot 10^{18}$  cm<sup>-2</sup> and  $\Delta v_{1/2}=15\pm 1$  km s<sup>-1</sup>. Due to the presence of the Galactic wings in the emission profiles, the size of the broad component is uncertain. Assuming that it

has a similar dimension as the narrow part, we have a volume density of  $\langle n \rangle=0.16\pm 0.07$  cm<sup>-3</sup> and pressure  $P=1151\pm 507$  K · cm<sup>-3</sup> for 116.2+23.6 and volume density  $\langle n \rangle=0.11\pm 0.04$  and  $P=535\pm 211$  K · cm<sup>-3</sup> for 115.0+23.9.

According to Rohlfs & Wilson (2004), assuming virialization, the line widths  $\Delta v_{1/2}$  of the H I clouds can be used to estimate their virial masses. For the H I clouds in Table 1 these calculations give typical virial masses  $M_{vir} \sim 10^4$  M<sub>⊙</sub>, which are more than two orders of magnitude larger than the visible H I masses listed there. This comparison indicates that the H I halo clouds observed with the Effelsberg telescope cannot be self-gravitating objects. Therefore an external confinement is needed for the clouds not to disperse. Assuming the presence of a hot halo according to Pietz et al. (1998) and Kalberla et al. (2007), the counterpart could be provided by the envelope and the surrounding hot halo medium. But in the cloud 116.2+23.6 its pressure  $P=14\pm 8$  K · cm<sup>-3</sup> is small in comparison to the envelope pressure of  $P=1151\pm 507$  K · cm<sup>-3</sup>. The same is true for the cloud 115.00+23.9, where the pressure for the cloud is  $P=19\pm 7$  K · cm<sup>-3</sup> in comparison to the pressure of the envelope of  $P=535\pm 211$  K · cm<sup>-3</sup>. In addition, a comparison of the H I cloud pressures  $P = \langle n \rangle \cdot T$  with theoretical estimates for warm component pressures from Wolfire et al. (2003) at the given Galactocentric radius range  $10 \lesssim R \lesssim 15$  kpc indicate a similar trend for the rest of the clouds of the sample. Before reaching a firm conclusion that the H I halo clouds may be transient objects, one can conclude that the clouds are unresolved. This implies that estimates for the sizes are upper limits only and higher resolution observations are needed.

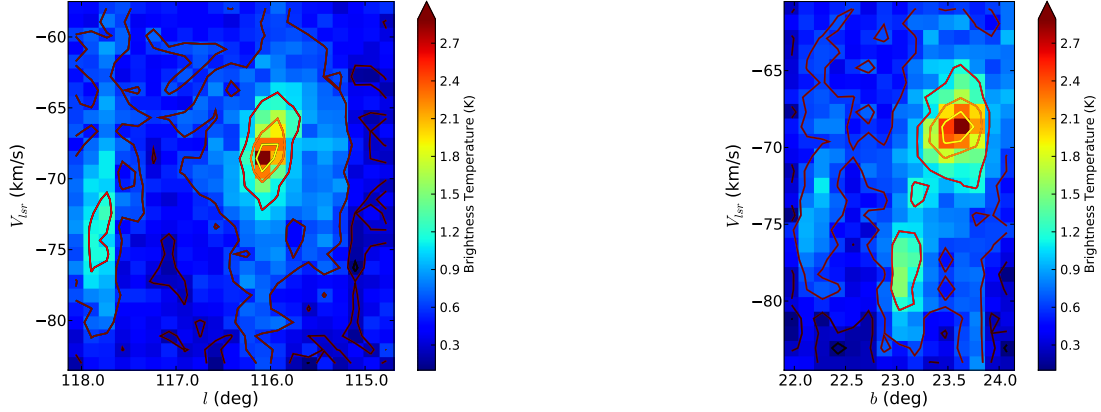


**Fig. 2.** Left: a) A longitude-velocity H I brightness temperature map of the cloud 116.20+23.55 taken by the Effelsberg 100-m telescope. The  $\sigma_n$  is 0.1K. The color-bar displays the transfer function. The contours are at 0.1, 0.3, 0.6, 0.9, 1, and 2 K. Right: b) A latitude-velocity H I brightness temperature map of the cloud 116.20+23.55 taken by the Effelsberg 100-m telescope. The  $\sigma_n$  is 0.1K. The color-bar displays the transfer function. The contours are at the level of 0.1K 0.3K 0.6K 0.9K 1K 2K.

#### 4.2. Synthesis observations

Two of the H I halo cloud positions from the Effelsberg sample were observed at high resolution to get a better constraint of the properties of the clouds. The first cloud 116.2+23.6 was observed with WSRT at a position (J2000)  $\alpha = 20^{\text{h}}4^{\text{m}}22^{\text{s}}$ ,  $82^{\text{d}}56'36''$  and has a line-of-sight velocity  $v_{l_{sr}} = -68 \text{ km s}^{-1}$ , which corresponds to a distance of  $d = 7 \text{ kpc}$  ( $R = 13 \text{ kpc}$ ,  $z = 2.5 \text{ kpc}$ ). It is cold with a line width  $\Delta v_{1/2} = 3 \text{ km s}^{-1}$  and a column density of  $N_{\text{HI}} = 11 \pm 2 \cdot 10^{18} \text{ cm}^{-2}$ . The second H I halo cloud, 115.0+23.9, was observed with VLA, at an offset position (J2000)  $(\alpha, \delta) = 20^{\text{h}}29^{\text{m}}$ ,  $82^{\text{d}}08'$  and has a line-of-sight velocity  $v_{l_{sr}} = -84.50 \text{ km s}^{-1}$ , which corresponds to a distance of  $d = 10 \text{ kpc}$  ( $R = 15 \text{ kpc}$ ,  $z = 4 \text{ kpc}$ ). This cloud shows also a narrow line width  $\Delta v_{1/2} = 3 \text{ km s}^{-1}$  and has a column density  $N_{\text{HI}} = 15 \pm 3 \cdot 10^{18} \text{ cm}^{-2}$ .

As seen in Fig. 3a a collection of compact H I objects was found in the WSRT observations at a  $v_{l_{sr}} = -68 \text{ km s}^{-1}$ . All cores with an angular radius  $s \geq 60''$  are significant at a signal-to-noise level of 5 or more. Some unexpected cores were found at a line-of-sight velocity of  $v_{l_{sr}} = -85 \text{ km s}^{-1}$  (Fig. 3 b). These are associated with an H I emission that is barely significant in the Effelsberg spectra. Similarly, at the position (J2000)  $(\alpha, \delta) = 20^{\text{h}}29^{\text{m}}$ ,  $82^{\text{d}}08'$ , observed with the VLA we find a conglomeration of at least 8 cores at a velocity of  $v_{l_{sr}} = -84 \text{ km s}^{-1}$  which are associated with the H I cloud 115.0+23.9. In Fig. 4 a channel map of the VLA observations is given.

In Table 2 median values for the observed quantities and derived physical parameters respectively are given for the H I cores detected with the WSRT and VLA telescopes. To determine the angular sizes and their column densities we produced separated 0th moment maps, and we fitted a 2D Gaussian. The fitted full width half maximum is the angular size  $s$  of the cores. From the integrated flux we estimated the column density. The line width is determined by inspection of the line since it was not possible to fit the spectra. Assuming a spherical shape, the average volume density is estimated. Finally for the pressure we used a similar method as the one described in Sec. 4.1. The H I cores show very narrow lines with a median of  $\Delta v_{1/2} = 3.3 \text{ km s}^{-1}$  and  $\Delta v_{1/2} = 4.3 \text{ km s}^{-1}$  for WSRT and VLA respectively, implying cold gas. The H I cores are also very compact with a median angular size  $s = 78''$  for WSRT and  $s = 88''$  for VLA, implying

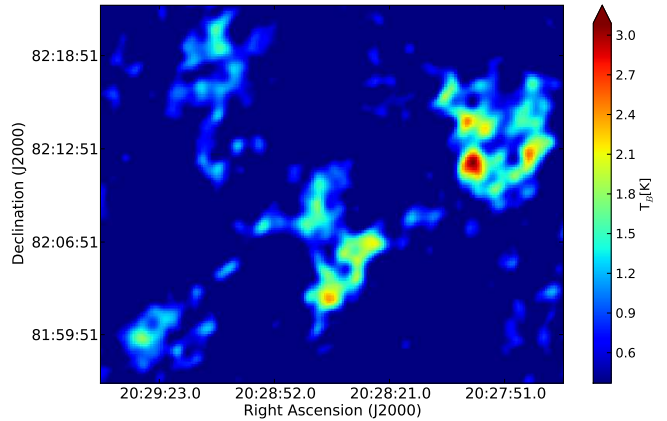


**Fig. 4.** An RA-DEC map of H I emission of the cloud 115.0+23.9 observed with VLA array centered at  $\alpha = 20^{\text{h}}29^{\text{m}}00^{\text{s}}$ ,  $\delta = 82^{\text{d}}08^{\text{m}}00^{\text{s}}$ ,  $v_{l_{sr}} = -84.50 \text{ km s}^{-1}$ . H I emission below the  $1\text{-}\sigma_n$  of 0.4K has been blanked out.

a median linear diameter of  $D = 2.6 \text{ pc}$  and  $D = 5 \text{ pc}$  respectively. For the measured column densities which are given in Table 2, the above diameters imply that the cores are a lot denser than what was estimated from the Effelsberg observations. For the H I cores detected with the WSRT, the median volume density is  $\langle n \rangle = 2.3 \pm 0.8 \text{ cm}^{-3}$ , while for the H I cores detected with the VLA the median is  $\langle n \rangle = 3.6 \pm 1.1 \text{ cm}^{-3}$ . A comparison of the total mass observed in the H I cores with the total visible H I mass of the “parent” Effelsberg cloud shows that they carry a large fraction of the mass. In the case of the WSRT cores they cover an area of  $15 \text{ arc-min}^2$  with a total mass of  $33 M_{\odot}$ , while the VLA cores cover an area of  $14.55 \text{ arcmin}^2$  and have a total visible H I mass of  $107 M_{\odot}$ . The H I cores have very small filling factors of 3%-4%, but carry a significant amount of the mass, up to 48% in comparison with the Effelsberg observations. The rest of the mass is associated most probably with the warmer H I envelope, which is extended and undetectable for an interferometer.

The high resolution interferometer observations enable us to determine accurately the morphology of the H I clouds observed with Effelsberg. They are resolved into individual H I cores for which kinematical pressures could be determined. As seen in

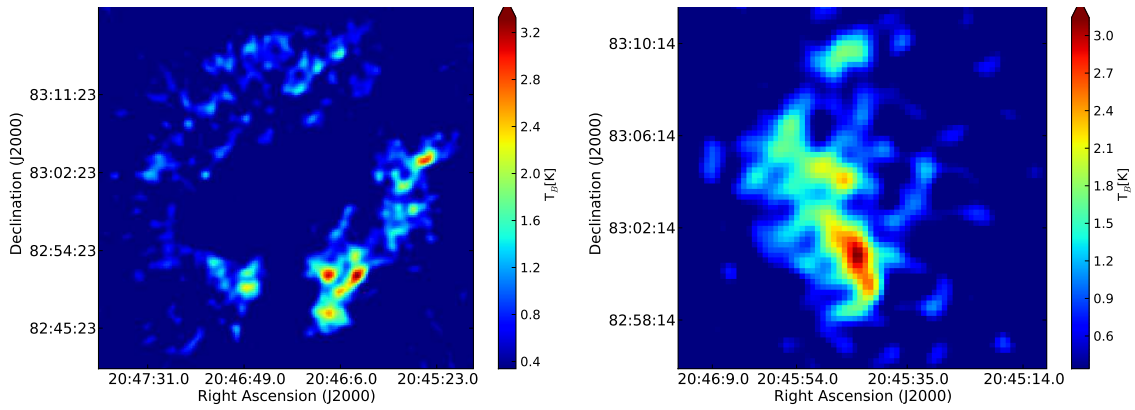


**Fig. 3.** a) A RA-DEC map of H I emission observed with the WSRT telescope centered at  $\alpha=20^{\text{h}}51^{\text{m}}00^{\text{s}}$ ,  $\delta=83^{\text{d}}01^{\text{m}}52^{\text{s}}$ ,  $v_{lsr}=-68.72$  km s $^{-1}$ . H I emission below the  $1-\sigma_n$  of  $=0.4\text{K}$  has been blanked out. b) An RA-DEC map of H I emission of the cloud 116.2+23.6 observed with the WSRT telescope centered at  $\alpha=20^{\text{h}}43^{\text{m}}48^{\text{s}}$ ,  $\delta=83^{\text{d}}04^{\text{m}}44^{\text{s}}$ ,  $v_{lsr}=-84.18$  km s $^{-1}$ . H I emission below the  $1-\sigma_n$  of  $0.4\text{K}$  has been blanked out.

**Table 2.** Derived parameters of the H I cores.

	$N_{HI}$ $10^{18} \text{ cm}^{-2}$	$s$ arcmin	$D$ pc	$T_{kin}$ K	$\langle n \rangle$ $\text{cm}^{-3}$	$P$ $\text{K} \cdot \text{cm}^{-3}$	$M_{HI}$ $M_{\odot}$
Range	12–32	58–127	1.9–5.9	140–350	1.3–3.1	270–980	1–24
Median	16	78	2.6	240	2.3	560	4
Range	29–76	54–124	2–6	170–730	2.2–5.7	780–2440	7–32
Median	40	86	5	410	3.6	1500	16

Note - The first two rows correspond to the cloud 116.2+23.6 observed with WSRT. The last two rows correspond to the cloud 115.0+23.9 observed with VLA.  $N_{HI}$  is the observed H I column density of the cores,  $s$  is the angular size,  $D$  is the spatial diameter.  $T_{kin}$  is the kinetic temperature.  $\langle n \rangle$  is the volume H I density.  $P$  is the pressure of the H I gas.  $M_{HI}$  is the visible H I mass of the core.

Table 2, the median pressure of  $P = 560 \pm 230 \text{ K}\cdot\text{cm}^{-3}$  for the WSRT sample and the median pressure of  $P = 1500 \pm 490 \text{ K}\cdot\text{cm}^{-3}$  for the VLA sample are both comparable within the uncertainties with the pressures of the surrounding envelope as estimated from the Effelsberg observation, which are  $P=1151\pm507 \text{ K}\cdot\text{cm}^{-3}$ , and  $P=535\pm211 \text{ K}\cdot\text{cm}^{-3}$  for the cloud observed with WSRT and VLA respectively.

A comparison of the pressures for cores and envelopes with theoretical estimates at different Galactocentric radii from Table 4 of Wolfire et al. (2003) shows that the derived quantities fit well to a two-phase picture with an approximate pressure equilibrium between the cores and the surrounding warm H I envelope. The envelopes as detected in the single dish observations (see Fig. 2) may provide the necessary support to stabilize the clouds. The envelope with a peak brightness temperature of  $\sim 0.8 \text{ K}$  is too weak to be detectable in our interferometer data. Additional deep observations would be needed to clarify the presence and extent of such a component. Nevertheless, combining the Effelsberg and WSRT/VLA observations can give us an insight into the nature of the ISM in the region of these clouds. Taking into account the presence of the very extended broad galactic wings, the warm envelope and the small scale cold cores which are unresolved with the Effelsberg telescope, we reach a sort of hierarchical structure of the ISM, similar to the turbulent flows found by Audit & Hennebelle (2005), which will be discussed later.

Using equation 47 from McKee & Cowie (1977) we can show that the envelope would protect the H I cores from fast evaporation. In the absence of a warm envelope, the mass loss for an H I core embedded in a hot plasma ( $T \sim 10^6 \text{ K}$ ) is  $\sim 7 \cdot 10^{-2} M_{\odot} \cdot \text{Myrs}^{-1}$ . This implies that a core with an average

mass of  $\sim 10 M_{\odot}$  will evaporate in  $\sim 140 \text{ Myrs}$ . A core embedded in a warm envelope ( $T \sim 7000 \text{ K}$  Wolfire et al. (2003)) has a mass loss of one magnitude smaller, on the order of  $\sim 6 \cdot 10^{-3} M_{\odot} \cdot \text{Myrs}^{-1}$ , and the cores will evaporate in  $\sim 1.7 \text{ Gyrs}$ . But because of internal turbulent motions the clouds will evolve within  $\sim 2 \cdot 10^5 \text{ yrs}$ . This is a very short time in comparison with the total time of their orbit, which is around  $100 \text{ Myrs}$ , which is found by simple ballistic simulation.

#### 4.3. Comparison between the properties of different samples of H I clouds

To better understand the physical properties of the H I halo clouds, but also in order to determine various systematics, it is reasonable to compare our clouds with different samples of H I clouds detected with other telescopes. The samples of clouds for a comparison are: a) Lockman (2002), where a population of clouds in the inner Galaxy ( $R \sim 3.5 \text{ kpc}$ ) was detected with GBT. The distance was determined using the terminal velocity of the sources. b) Stanimirović et al. (2006), using the Arecibo 300-m radio telescope, detected a number H I clouds distinctively separated from the Galactic disk towards the anti-center direction. Due to high intrinsic uncertainties, kinematic distances were not used, and the authors opted to use pressure equilibrium considerations to determine the distance. c) Ford et al. (2008), where a large number of H I clouds were detected within the pilot region of the Galactic All-Sky Survey (GASS) with the Parkes 64-m telescope. The terminal velocity was used as well to determine the distance, since the clouds are located in the inner Galaxy. d) Stil et al. (2006), where in the VLA Galactic Plane Survey

(VGPS) 17 fast moving H I clouds were detected close to the plane which are possibly associated with the halo gas phase.

An inter-comparison of the main results from these authors is given in Table 3. Telescope independent quantities, like  $N_{\text{HI}}$  and  $\Delta v_{1/2}$ , are found to be similar, with an exception of  $N_{\text{HI}}$  from Stil et al. (2006); the higher column densities in this sample can be explained by the low altitude of the sample. The other cloud properties are similar, which may imply that the different cloud samples in the inner and the outer Galaxy may have a similar origin.

The telescope-dependent properties of the samples,  $s$ ,  $D$ ,  $n$ ,  $M_{\text{HI}}$ , show a different picture. Telescopes with similar resolutions, like Effelsberg, GBT and Parkes, show similar ranges for  $s$ ,  $D$ ,  $\langle n \rangle$ ,  $M_{\text{HI}}$ . Taking into account that the source distances are fairly similar, it is quite clear that the telescope used in each work may introduce a twofold systematic bias: a) Synthesis telescopes work as spatial filters, more sensitive to cold compact than to warm extended gas. b) The measured angular diameter  $s$  depends on the convolution of the actual cloud size  $s_t$  and the beam size. As such the  $s_t$  is overestimated, leading to an underestimate of the measured volume density  $n$ . For the same cloud, telescopes with increased resolution will either resolve the cloud or measure  $s$  closer to the  $s_t$ . Therefore the errors in the determination of the parameters depending on the angular size such as  $D$ ,  $n$ ,  $M_{\text{HI}}$  are smaller, and the measurements are closer to the properties of the clouds. This dependence on the beam size obviously explains that the Arecibo observations (beam resolution  $\sim 4'$ ) yield parameters for the clouds closer to the ones estimated for the H I cores observed with the WSRT and the VLA telescope.

## 5. Discussion

In Sect. 4.2 we found indications for a pressure equilibrium between the H I cores which constitute the halo clouds and the warmer envelopes in which they are possibly embedded. In the Galactic disk, it has been shown (see Wolfire et al. 2003, and reference therein) that the two main phases, the cold medium phase with  $T \sim 100\text{K}$  and the warm medium phase (WNM) with  $T \sim 10^4\text{K}$  (Kulkarni & Heiles 1987), can co-exist in pressure and thermal equilibrium only in a very narrow range of pressures and densities. The Wolfire et al. (2003) model determines this range for different Galactocentric distances up to  $R = 18\text{kpc}$ . The model takes into account various observational constraints, e.g. dust and metallicities; for a more detailed discussion see Chap.2 and 3 of Wolfire et al. (2003). It is assumed that the main heating for the neutral medium originates from the dust grains through the FUV of young stars. The cooling of the cold phase is mainly due to the fine-structure of the C II line ( $158\mu\text{m}$ ), while the cooling of the warm phase happens in through the Ly $\alpha$ , C II ( $158\mu\text{m}$ ) and O I ( $63\mu\text{m}$ ), with the electron recombination mechanism also playing an important role. It is important to note here that the model depends on the dust-to-gas ratios, the metallicity and the assumed FUV field (Wolfire et al. 1995).

Since we were able to determine the volume densities of the H I gas  $\langle n \rangle$  and the pressure  $P$  for the halo clouds and the cores, it is worth comparing the phase diagrams as estimated by Wolfire et al. (2003) with our results. We make the following assumptions:

1. In Wolfire et al. (2003) it is assumed that the total density of the hydrogen nucleus is  $n_H = n_{\text{HI}} + n_{\text{H}_2}$  where  $n_{\text{HI}}$  is the spatially averaged volume H I density and  $n_{\text{H}_2}$  is the spatially

averaged molecular hydrogen density. Up to now no direct CO observation of the H I halo clouds has been done, therefore their molecular content is unknown and we assume that  $n_H = n_{\text{HI}}$ .

2. The H I halo clouds detected in this work are located at a height of  $1 \lesssim z \lesssim 5$  kpc above the plane. According to Eq. 4 from Wolfire et al. (1995), which gives the height dependence of the FUV field, the FUV for  $z = 5$  kpc is similar to the FUV field in the plane ( $z = 0$ ). Therefore, for dust-to-gas ratios and metallicities similar to the plane, we can use the phase diagrams from Wolfire et al. (2003) estimated for the plane ( $z = 0\text{kpc}$ ).

In Fig. 5a we compare the properties of the H I cores observed with the VLA/WSRT with the theoretical phase diagrams. The envelope estimates in this plot are given from the Effelsberg observations described in Sec.4.1 As discussed in Sec. 4.2, the H I cores of the VLA have a  $R \sim 15$  kpc, while the WSRT cores have an estimated  $R$  from 13 kpc up to 15 kpc. As seen in the Fig. 5a, at the corresponding  $R$  the WSRT cores with  $v_{\text{lsr}} = -68 \text{ km s}^{-1}$  are located barely within the range where thermal equilibrium is possible and cold gas can exist in a stable phase. For the WSRT cores at  $v_{\text{lsr}} = -84 \text{ km s}^{-1}$ , some are located in the thermally unstable region, while others have volume densities matching the expectations for the CNM, with smaller pressures than the ones expected for the CNM at  $R=15$  kpc. For some of the VLA cores in Fig. 5a we find pressures which are higher than expected for cold gas in the equilibrium.

The derived pressures, plotted in Fig. 5a, may be biased. As described in Sec.4.1 they were derived from  $P = \langle n \rangle \cdot T_{\text{kin}}$ . The uncertainties are difficult to estimate. The kinetic temperature is most probably an upper limit, while the volume density  $\langle n \rangle$  is affected by distance uncertainties, beam smearing and geometry of the source. Distance uncertainties should be on the order of 20%. Beam smearing may cause overestimates of the source extension, but more importantly may be biases caused by the geometry of the source. If these clouds have a sheet-like structure (Heiles & Troland 2003) we may seriously underestimate the volume density and accordingly the pressure. Both sources show a very narrow line width. Assuming the typical spin temperature in the range of 40 to 80 K, resulting biases should be within a factor of a few times. Volume densities of the cores may be more seriously biased. Taking this into account, the true position of the cores in Fig. 5a could possibly be in better agreement with the cold branch.

Regarding the position of the cores in the phase diagram, one other important detail is that their molecular gas content is unknown. Recent absorption experiments report some low column density molecular hydrogen in small (0.1pc) and dense clumps in the Milky Way halo with H I column densities  $N_{\text{HI}} > 10^{19}$  (Richter 2005). Such possible biases imply that the cold gas in the H I cores can be well in thermal equilibrium with the surrounding warmer gas, detected in the single dish observations, which then would play the role of a confining envelope.

The position of the H I cores in the phase diagram is explained in the above section, using a simplified static thermal equilibrium hypothesis between the two components of the ISM. Non-thermal effects such as turbulence or magnetic fields are not taken into account. Recent numerical simulations (Gazol et al. 2005; Audit & Hennebelle 2005) examine the influence of non-thermal factors. As a result, the positions of the H I cores in the phase diagram (Fig. 5a) and their origins can be explained in the context of a dynamical equilibrium under the influence of tur-

**Table 3.** A comparison between the H I halo cloud samples observed with different telescopes.

	$ z $ kpc	$d$ kpc	$N_{\text{HI}}$ $10^{19}\text{cm}^{-2}$	$\Delta v_{1/2}$ $\text{km s}^{-1}$	$s$ '	$D$ pc	$\langle n \rangle$ $\text{cm}^{-3}$	$M_{\text{HI}}$ $M_{\odot}$
Effelsberg	0.9–5.4	3–11	0.4–7.4	2–21.1	9–27	8–70	0.07–1.2	3–770
WSRT			1.2–3.2	2.5–4.0	0.9–2.1	2–6	1.3–3.1	1–24
VLA			2.9–7.6	2.8–5.8	0.9–2.1	2–6	2.2–5.7	7–32
Lockman (2002)	0.6–1.2		0.7–6.3	5.4–26.3		19–35	0.1–0.9	12–290
Stanimirović et al. (2006)	0.06–0.9	0.2–3	1–3	3–7.6	6–12	0.6–8		0.03–7
Ford et al. (2008)	0.3–1.7		0.2–2.2	5.8–26.2		46–100		120–4850
Stil et al. (2006)	0.01–0.16	4.2–7.7	8–39	3.4–16.5	1.8–29.4	3.4–36.7	3–24	9–2500

Note - The table gives the range of values of the clouds for the following properties:  $|z|$  which is the absolute height above the plane (defined in the inner part of the disk) in kpc.  $d$  the distance in kpc.  $N_{\text{HI}}$  is the column density of H I gas in  $10^{19}\text{cm}^{-2}$ .  $\Delta v_{1/2}$  is the line width in  $\text{km s}^{-1}$ .  $s$  is the observed angular size in '.  $D$  is the diameter in pc.  $\langle n \rangle$  is the average volume density in  $\text{cm}^{-3}$ .  $M_{\text{HI}}$  is the visible H I mass in  $M_{\odot}$ .

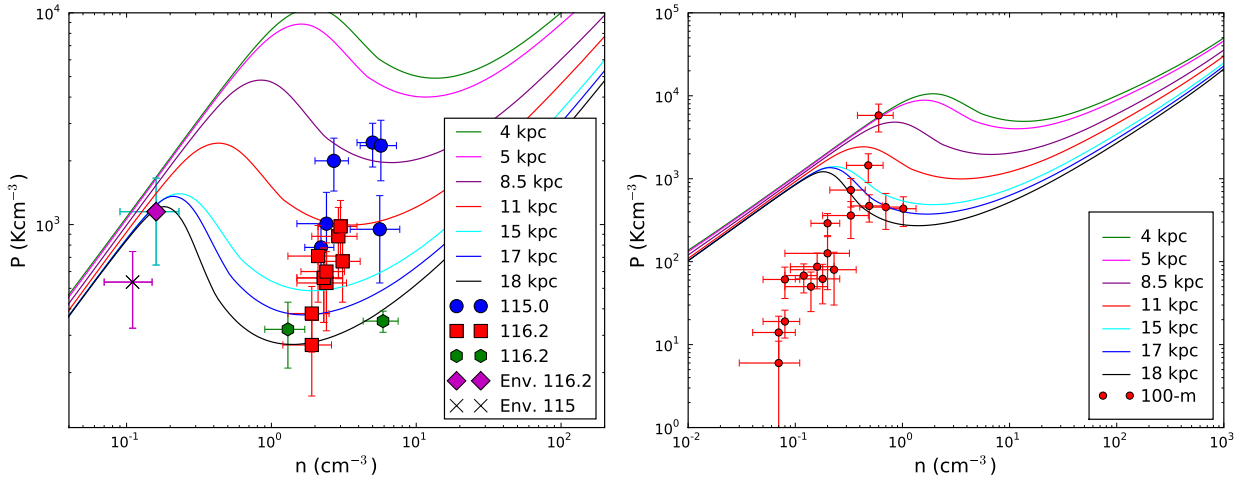


**Fig. 5.** a) Parameters derived from the WSRT & VLA samples. The envelope pressure is determined by the Effelsberg observations. The curves in both plots apply to column densities of the order of  $10 \cdot 10^{18} \text{cm}^{-2}$  b) A comparison between the Effelsberg sample of H I clumps and the phase diagrams depicting thermal pressure  $P/k$  vs. hydrogen nucleus density  $n$  at different Galactocentric radii (Wolfire et al. 2003).

bulence. Audit & Hennebelle (2005) examine the influence of turbulence in a converging flow of WNM. Under the influence of the turbulent velocity field, warm gas is forced out of thermal equilibrium into the unstable regime. In this part of the phase diagram, the gas forms cold condensations, which are connected by less dense structure.

The more turbulent the gas, the larger the fraction of the gas which is driven in the intermediate unstable region of the phase diagram (see for comparison in Figs. 3 and 7 of Audit & Hennebelle (2005)). A very turbulent flow, also part of their simulation, generates more complex structures, and in addition cold structures are significantly less dense, even at intermediate densities around  $\langle n \rangle \sim 5\text{cm}^{-3}$ . Interestingly, this is quite similar to the volume densities we observe in the H I cores (Table 2). A comparison of the density field and the interferometry maps (Figs. 3–4) shows a comparable morphology.

Similar numerical experiments of Gazol et al. (2005) study the behavior of a bistable gas flow under the influence of a turbulent velocity field and model gas that is driven into the unstable region. It is shown that as either the effective Mach number  $M$  or the driving scale increases, a departure of the gas from thermal equilibrium is observed, approaching an adiabatic behavior. What is interesting in comparison with the phase diagrams presented in this work is that a population of under-pressured zones is generated in the diffuse gas, while in the dense gas over-pressured zones are created. Although, as

mentioned before, the simulations do not represent an accurate model of the ISM, this trend is probably seen in the phase diagrams of Fig. 5a. All in all, it seems that the positions of the H I cores in the phase diagram agree with the predictions above, implying that turbulence strongly affects the state of the halo ISM. The H I halo clouds are probably transient filamentary features, cold unstable gas which is continuously condensing out of the WNM, a process that is caused by turbulence and is stabilized by it. This result fits well to the finding that the extra-planar gas in general is strongly affected and supported by turbulence (Kalberla & Kerp 1998).

A comparison of Fig 5a, derived from interferometer data, with Fig. 5b, using single dish data only, shows huge differences. Parsec sized H I clumps are unresolved by single dish telescopes, estimates for pressures and densities appear seriously biased in this case. Interferometers on the other hand are insensitive for the extended envelopes which appear to surround cold HI cores. The ideal telescope should resolve both, the extended features as well as compact cores. Within a few years the Australian Square Kilometer Array Pathfinder (ASKAP) may be able to satisfy both demands, providing a large number of sources in intermediate and high latitudes for a comparison with theoretical models of the multi phase ISM.

## 6. Conclusion

We discussed a population of H I clouds residing in the lower halo of the Milky Way, co-rotating with the Galactic disk. The sample was observed with the 100-m Effelsberg telescope. Search criteria were angular sizes  $s$ , the brightness temperatures  $T_B$  and line width  $\Delta v_{1/2}$  which are considered to be typical for halo clumps. The sample includes H I clumps with the following properties:

- they reside in the outer galaxy with Galactocentric radii  $R$   $10 < R < 15$  kpc.
- they belong to the lower halo ( $0.9 < z < 5.4$  kpc).
- the gas is cold, with a median  $T_{kin} \sim 600$  K and a line width  $\Delta v_{1/2} = 5.3 \text{ km s}^{-1}$ .
- the sample shows a prominent two-component structure. Cold H I cores are surrounded by an extended component with broad line emission.

Two of the most prominent H I clouds were observed using synthesis arrays, the WSRT and the VLA. These high-resolution observations resolve the clouds into a conglomeration of arcminute sized H I cores. These cores are embedded in a more diffuse medium which is detectable only with single dish telescopes. The cores contain a significant fraction of the H I mass and tend to be in pressure equilibrium with the surrounding envelopes. Taking into account the influence of turbulence onto the line widths  $\Delta v_{1/2}$ , the median line width values of  $3.3 \text{ km s}^{-1}$  and  $4.3 \text{ km s}^{-1}$  observed at the cores implies that the H I gas is very cold.

Estimating densities and pressures for clumps and surrounding envelopes, we find some scattering but also a reasonable agreement with models which predict pressure equilibrium and a multi-phase structure caused by thermal instabilities (Wolfire et al. 2003). The clumps tend to populate unstable regions in the phase diagrams, in agreement with recent predictions of turbulence driven instabilities (Audit & Hennebelle 2005; Gazol et al. 2005).

Comparing samples observed with big single dish telescopes e.g. GBT (Lockman 2002), Effelsberg (this work), and Parkes (Ford et al. 2008), we find similar column densities, peak temperatures, line widths and masses. Our interferometer observations imply that some of the derived parameters may be heavily biased if the small scale structure observed by us may be considered as typical for H I halo clumps.

*Acknowledgements.* This publication is based on observations with the 100-m telescope of the MPIfR (Max-Planck-Institut für Radioastronomie) at Effelsberg. For the introduction we made use of comments from W. B. Burton concerning early observations of the halo gas phase that we received as a response to a previous publication. The project was supported by the *Deutsche Forschungsgemeinschaft*, DFG project number KA1265/5-2. Leonidas Dedes would like to thank Karl Menten for his support and Endrik Kruegel for his useful corrections. Finally the authors would like to thank the anonymous referee for the his helpful comments.

## References

Audit, E. & Hennebelle, P. 2005, *A&A*, 433, 1  
 Brand, J. & Blitz, L. 1993, *A&A*, 275, 67  
 Burton, W. B. & Liszt, H. S. 1983, *A&AS*, 52, 63  
 Clark, B. G. 1980, *A&A*, 89, 377  
 Dickey, J. M. & Lockman, F. J. 1990, *ARA&A*, 28, 215  
 Ford, H. A., McClure-Griffiths, N. M., Lockman, F. J., et al. 2008, *ApJ*, 688, 290  
 Gazol, A., Vázquez-Semadeni, E., & Kim, J. 2005, *ApJ*, 630, 911  
 Gómez, G. C. 2006, *AJ*, 132, 2376  
 Hartmann, D. & Burton, W. B. 1997, *Atlas of Galactic Neutral Hydrogen (Atlas of Galactic Neutral Hydrogen, by Dap Hartmann and W. Butler Burton,*

pp. 243. ISBN 0521471117. Cambridge, UK: Cambridge University Press, February 1997.)  
 Heiles, C. & Troland, T. H. 2003, *ApJ*, 586, 1067  
 Kalberla, P. M. W. & Dedes, L. 2008, *A&A*, 487, 951  
 Kalberla, P. M. W., Dedes, L., Arnal, E. M., et al. 2005, in *Astronomical Society of the Pacific Conference Series*, Vol. 331, *Extra-Planar Gas*, ed. R. Braun, 81–+  
 Kalberla, P. M. W., Dedes, L., Kerp, J., & Haud, U. 2007, *ArXiv e-prints*, 704  
 Kalberla, P. M. W. & Kerp, J. 1998, *A&A*, 339, 745  
 Kalberla, P. M. W., Mebold, U., & Reich, W. 1980, *A&A*, 82, 275  
 Kalberla, P. M. W., Westphalen, G., Mebold, U., Hartmann, D., & Burton, W. B. 1998, *A&A*, 332, L61  
 Kulkarni, S. R. & Heiles, C. 1987, in *Astrophysics and Space Science Library*, Vol. 134, *Interstellar Processes*, ed. D. J. Hollenbach & H. A. Thronson, Jr., 87–122  
 Levine, E. S., Blitz, L., & Heiles, C. 2006, *ApJ*, 643, 881  
 Lockman, F. J. 1984, *ApJ*, 283, 90  
 Lockman, F. J. 2002, *ApJ*, 580, L47  
 Lockman, F. J. & Gehman, C. S. 1991, *ApJ*, 382, 182  
 McKee, C. F. & Cowie, L. L. 1977, *ApJ*, 215, 213  
 Oort, J. H. 1962, in *The Distribution and Motion of Interstellar Matter in Galaxies*, ed. L. Woltjer, 71–+  
 Pietz, J., Kerp, J., Kalberla, P. M. W., et al. 1998, *A&A*, 332, 55  
 Richter, P. 2005, in *Astronomical Society of the Pacific Conference Series*, Vol. 331, *Extra-Planar Gas*, ed. R. Braun, 41–+  
 Rohlfs, K. & Wilson, T. L. 2004, *Tools of radio astronomy (Tools of radio astronomy, 4th rev. and enl. ed., by K. Rohlfs and T.L. Wilson. Berlin: Springer, 2004)*  
 Shane, W. W. 1967, in *IAU Symposium*, Vol. 31, *Radio Astronomy and the Galactic System*, ed. H. van Woerden, 177–+  
 Shane, W. W. 1971, *A&AS*, 4, 315  
 Simonson, III, S. C. 1971, *A&A*, 12, 136  
 Stanimirović, S., Putman, M., Heiles, C., et al. 2006, *ApJ*, 653, 1210  
 Stark, A. A., Gammie, C. F., Wilson, R. W., et al. 1992, *ApJS*, 79, 77  
 Stil, J. M., Lockman, F. J., Taylor, A. R., et al. 2006, *ApJ*, 637, 366  
 Takakubo, K. 1967, *Bull. Astron. Inst. Netherlands*, 19, 125  
 Weaver, H. & Williams, D. R. W. 1973, *A&AS*, 8, 1  
 Wolfire, M. G., McKee, C. F., Hollenbach, D., & Tielens, A. G. G. M. 1995, *ApJ*, 453, 673  
 Wolfire, M. G., McKee, C. F., Hollenbach, D., & Tielens, A. G. G. M. 2003, *ApJ*, 587, 278